Numerical simulations of sand migration in interbedded hydrate-bearing sediments at Site NGHP-02-16

Shun Uchida[a,b,*], Jeen-Shang Lin[c,b], Evgeniy M. Myshakin[b], Yongkoo Seol[b], Timothy S. Collett[d], Ray Boswell[b]

[a] *Rensselaer Polytechnic Institute*
[b] *U.S. Department of Energy, National Energy Technology Laboratory*
[c] *University of Pittsburgh*
[d] *U.S. Geological Survey*

Abstract

The geomechanical behavior of hydrate-bearing sediments during gas production is complex, involving changes in hydrate-dependent mechanical characteristics and also redistribution of stresses carried by hydrates. When an interbedded mud layer is present, the complex response of the hydrate-bearing sediments is more pronounced because hydrate dissociation tends to occur preferentially in the sediments adjacent to the mud layer due to available heat source. This leads to non-uniform sediment deformation and potentially shearing deformation along the sand/mud layers. In addition, since the sediment permeability is also hydrate-dependent, a greater pressure gradient may exist along the sand/mud layers. These two tendencies may contribute to sand migration, which hindered the past field-scale gas production tests, and thus a thorough study on the effect of a thin interbedded mud layer on the extent of sand migration is necessary. This paper presents numerical sand migration modeling of sand/mud interbedded hydrate-bearing sediments found at Site NGHP-02-16 subjected to depressurization. For a comparison and better understanding, simulation of homogenous hydrate-bearing sediments is also conducted. It is found that greater sand migration occurs when the interbedded mud layer is present because of shearing deformation and greater pressure gradient along the sand/mud layer. Although the magnitude may vary with values of sand migration related parameters, this finding implies that there would be a greater potential of sand migration at Site NGHP-02-16 where the production zone consists of a number of sand/mud interbedded layers.

Keywords: sand migration, hydrate-bearing sediments, shearing deformation

*Corresponding author
Email address: uchids@rpi.edu (Shun Uchida)

1. Introduction

For a successful long-term gas production from gas hydrate-bearing sediments in the field, it is essential to better understand the responses of the sediments during gas extraction. Gas hydrate-bearing sediments undergo highly coupled multiphysics changes in thermal, hydrological and mechanical characteristics when subjected to depressurization. In previous field-scale gas hydrate production tests, the sediments exhibited uncontrolled sand migration into the well, resulting in premature termination of the well tests (Dallimore et al., 2012; Yamamoto et al., 2014). Motivated by these incidents, Uchida et al. (2016a) developed an analytical thermo-hydro-mechanical sand production model in gas hydrate-bearing sediments and showed the responses of simple homogenous hydrate-bearing sediments subjected to depressurization. Since hydrate-bearing sediments in real fields are not homogeneous, this paper investigates the responses of more representative hydrate-bearing sediments, in particular, sand/mud interbedded hydrate-bearing sediments through near-wellbore-scale numerical sand migration modeling. The setting is typically found at Site NGHP-02-16 and the conditions considered in this study correspond to a large-scale reservoir model for Site NGHP-02-16 presented in Myshakin et al. (2017). The mechanical behavior of the sediments at the site is modeled based on a series of geomechanical tests on the pressure cores recovered from the site (conducted by Yoneda et al. (2017)), which are also used for a large-scale modeling of geomechanical stability assessment by Lin et al. (2017). The parameters for the sand migration model are based on the past field test of gas production from hydrate-bearing sediments (Uchida et al., 2016b). Consequently, the results may be deemed best possible estimate of the quantity of sand migration at Site NGHP-02-16 but the focus of this study is to qualitatively investigate the effect of thin mud layer within sandy hydrate-bearing sediments on sand migration.

This paper consists of four sections. Firstly, a brief summary of the thermo-hydro-mechanical sand migration model by Uchida et al. (2016a) is presented. Secondly, the near-wellbore-scale model utilized for this study including the initial conditions and geomechanical properties is summarized. Thirdly, the results of sand migration analyses both with and without the presence of mud layer are presented. The final section summarizes the key findings.

2. Overview of thermo-hydro-mechanical sand migration model

This study adopts the thermo-hydro-mechanical sand migration model developed by Uchida et al. (2016a). The model treats sand migration roughly in three stages: (a) detachment (or mobilization); (b) migration and (c) flowing into a well. First, sand particles are detached from soil skeletal continuum due to high hydraulic gradient exceeding its critical value. Secondly, the detached particles travel with pore fluid (water and/or gas) at the same superficial velocities, constituting sand-fluid mixtures. Thirdly, the migrating particles may settle or settled particles may be lifted and only the sand particles flowing into a well

are considered as sand production. These stages are schematically illustrated in Fig. 1.

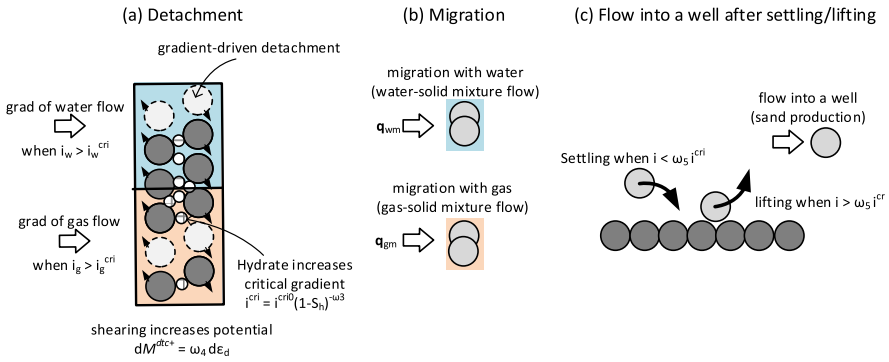

Figure 1: Stages considered in sand migration model

In the first stage, when sand particles are detached from a part of soil skeletal continuum, it is assumed to temporarily cause the effective stress reduction (soon to be fully or partially recovered by mechanical deformation). The extent of reduction in the effective stresses is assumed to depend on the amount of detached sand particles and also the effective stresses carried by the soil skeleton. This mechanical-particle detachment coupling is governed by a parameter ω_1 as:

$$\frac{\partial \boldsymbol{\sigma}'}{\partial V_{ssi}} dV_{ssi} = \omega_1 \boldsymbol{\sigma}' \frac{dV_{ssi}}{V_{ssi}} \tag{1}$$

where $\boldsymbol{\sigma}'$ is the effective stress tensor represented in a vector form and V_{ssi} is the volume of intact sand forming skeletal continuum and dV_{ssi} is the volume of detached sand particles (negative denotes detachment). The actual detachment occurs when the hydraulic gradient of water and/or gas exceeds its critical value. The detached volume is controlled by the amount of intact solids and detachability potential M^{dtc} (discussed later) such that:

$$dV_{ssi} = -\omega_2 V_{ssi} M^{dtc} \left(\frac{S_w}{S_w + S_g} H_w + \frac{S_g}{S_w + S_g} H_g \right) dt \tag{2}$$

where ω_2 is the parameter incorporating rate (time^{-1}), S is the saturation, $H_w = H\left(\frac{i_w}{i_w^{crit}} - 1\right)$, $H_g = H\left(\frac{i_g}{i_g^{crit}} - 1\right)$, $H(x)$ is the heaviside step function, i is the size of hydraulic gradient vector (i.e. $i = |\mathbf{i}|$), i^{crit} is the critical hydraulic gradient above which detachment of a sand particle occurs, t is the time and the subscripts w and g represent water and gas, respectively. The relative pore occupancy in front of H_w and H_g facilitates the proportionality between water-driven and gas-driven detachment, respectively. The critical hydraulic gradient is assumed to increase with hydrate saturation as hydrates may resist

detachment through supporting neighboring sand particles and the suggested model utilizes the power function with a parameter ω_3:

$$i^{crit} = i^{crit0}(1 - S_h)^{-\omega_3} \tag{3}$$

where i^{crit0} is the critical hydraulic gradient for particle detachment under single-phase (no hydrate) condition and S_h is the hydrate saturation. The detachability potential introduced in Eq. (2) incorporates the effect of shearing deformation of the soil skeleton and a parameter ω_4 converts the strain value to the detachability potential by:

$$M^{dtc} = \omega_4 \epsilon_d + \ln\left(\frac{V_{ssi}}{V_{s0}}\right) \tag{4}$$

where ϵ_d is the deviatoric strain and V_{s0} is the initial intact sand volume (= V_{ssi0}). This model implies that sand particle detachment only occurs when there has been shearing deformation and it ceases when the potential becomes zero (i.e., $M^{dtc} = 0$) even if the hydraulic gradient is above its critical value.

The detached particle are mobilized and transport with the driven-fluid (water and/or gas) forming sand-fluid mixtures according to the Darcy's law. This is the second stage of the model, describing sand migration. The state of sand particles that are currently flowing is denoted as the subscript fs and its volume is given by the summation of flowing sand particles in sand-water mixture (noted as $fs|wm$) and those in sand-gas mixture (noted as $fs|gm$):

$$V_{fs} = V_{fs|wm} + V_{fs|gm} \tag{5}$$

where the subscripts wm and gm are for the sand-water mixture (i.e., $V_{wm} = V_{fs|wm} + V_w$) and the sand-gas mixture (i.e., $V_{gm} = V_{fs|gm} + V_g$).

In the third stage, the flowing sand particles may settle when the hydraulic gradient becomes lower than $\omega_5 i^{crit}$(where $0 \leq \omega_5 \leq 1$) or settled ones may be lifted again when the hydraulic gradient becomes greater than $\omega_5 i^{crit}$, that is:

$$\begin{aligned} \frac{dV_{sst}}{dt} &= V_{fs|wm}(1 - H_{w5}) + V_{fs|gm}(1 - H_{g5}) \\ &\quad -V_{sst}\left(\frac{S_w}{S_w + S_g}H_{w5} + \frac{S_g}{S_w + S_g}H_{g5}\right) \end{aligned} \tag{6}$$

where $H_{w5} = H\left(\frac{i_w}{\omega_5 i_w^{crit}} - 1\right)$, $H_{g5} = H\left(\frac{i_g}{\omega_5 i_g^{crit}} - 1\right)$, V_{sst} is the settled sand particles in which the particles are stationary but not part of soil skeleton, leading to no effective stresses change upon settling/lifting. The overall sand volume is therefore given by $V_s = V_{ssi} + V_{sst} + V_{fs}$. The first two terms of the right-hand side of Eq. (6) represent settling and the last term denotes lifting requiring the relative pore occupancy term.

In total, the thermo-hydro-mechanical sand migration model requires six parameters. Table 1 summarizes their symbols, physical meaning, corresponding equation number and also the values adopted for the parameters. The values are based on the simulations of the 2013 Nankai gas production test (Uchida et al., 2016b) which showed fairly well history matching of the overall produced sand volume as well as gas and water production.

Table 1: Sand production model parameters

Symbol	Description	Eq. number	Values
ω_1	Stress reduction by detachment	Eq. (1)	2.0
ω_2	Rate of detachment	Eq. (2)	0.1 hr^{-1}
ω_3	Critical gradient increase with hydrate	Eq. (3)	3.0
ω_4	Shearing to potential conversion	Eq. (4)	1.0
ω_5	Settling/lifting	Eq. (6)	0.5
i^{crit0}	Critical gradient under single-phase	Eq. (3)	5.0

3. Near-wellbore-scale numerical model for Site NGHP-02-16

3.1. Model geometry and initial conditions

While reservoir-scale models for Site NGHP-02-16 may be ideal, due to computational limitation, the thermo-hydro-mechanical sand migration model is better suited for a smaller scale. Therefore, this study employs near-wellbore-scale modeling approach, focusing on, rather than the whole Site NGHP-02-16 or entire hydrate-bearing sand, a thin hydrate-bearing sand with its bounding mud layers that alternately exist in Unit 4 as shown in Fig. 2. Gas production prediction and sea floor subsidence prediction at the site have been conducted in a reservoir-scale and these can be found in Myshakin et al. (2017) and Lin et al. (2017), respectively. The focused layer for this sand migration study is assumed to be located 2850 m from the sea level and 280 m from the sea floor, leading to the initial pore pressure and effective vertical stress of $P_{w0} = 28.5$ MPa and $\sigma_{z0} = 2.8$ MPa, respectively. The initial temperature is $T_0 = 19.4$ °C and the well is assumed to be insulated. Hydrates are assumed to exist only in the sand layer, forming homogeneous hydrate-bearing sand, and the initial hydrate saturation is $S_{h0} = 80$ %.

The top and bottom sides of mechanical boundary is roller supported (i.e. smooth in the radial direction), facilitating a periodic boundary condition to incorporate the existence of hydrate-bearing sediments above and below. This leads to no thermo-hydraulic flow at the top and bottom sides of the boundary and thus convection and conduction are only from the far-field boundary (i.e. far right-hand side in Fig. 2c) where the pore pressure and temperature remain constant. The wellbore boundary is mechanically-fixed in both directions but open for gas, water and sand productions. The far-field boundaries are total stress controlled, that is, both the pore pressure and effective radial stress remain constant, which are in this study $P_{w0} = 28.5$ MPa and $\sigma_{r0} = 1.4$ MPa, respectively. The size of the wellbore is $r_0 = 0.15$ m and the far-field boundary is set at $r_\infty = 50$ m. The domain is discretized into 30 elements in the radial direction, spanning the radial size from approximately 0.1 to 10 m.

3.2. Geomechanical and other physical properties

For modeling of geomechanical behavior of hydrate-bearing sand in Unit 4, this study utilizes the methane hydrate critical state constitutive model (Uchida

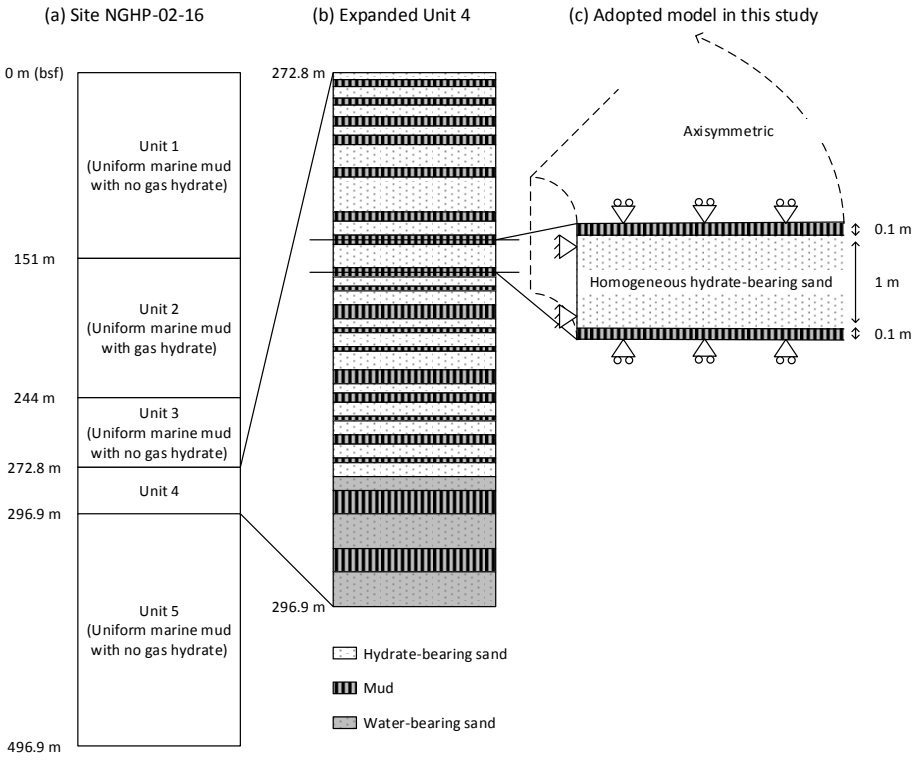

Figure 2: Schematic geometry of (a) Site NGHP-02-16; (b) Unit 4; and (c) the model used in this study

Table 2: Mechanical and hydrological parameters adopted in this study

Mechanical	Sand	Mud
Critical state friction M	1.2	1.3
Slope of compression λ	0.087	0.20
Slope of swelling κ	0.011	0.05
Preconsolidation stress p'_{cs}	2.6 MPa	3.9 MPa
Subloading factor u	1	960
Mechanical hydrate saturation S_h^{mec}	$\exp\left(-\epsilon_d^p\right) S_h$	–
Cohesion enhancement p'_{cc}	$2\left(S_h^{mec}\right)^{1.1}$	–
Dilation enhancement p'_{cd}	$10\left(S_h^{mec}\right)^{2.0}$	–
Hydrological	**Sand**	**Mud**
Initial porosity n_0	0.4	0.4
Initial hydrate saturation S_{h0}	0.8	0
Initial intrinsic permeability $\|\|\mathbf{K}\|\|$	1000 mD	0.05 mD
Initial effective permeability $\|\|\mathbf{K}_h\|\|$	1 mD	0.05 mD

et al., 2012). The model captures both shear yielding and volumetric yielding, the latter is particularly important under depressurization scheme. The model is calibrated against a series of geomechanical tests by Yoneda et al. (2017) on the pressure core samples recovered from Site NGHP-02-16. The detailed model description as well as fitting procedure are provided in Lin et al. (2017). One of the key findings regarding the hydrate-bearing sand at the site is that it appears to be rather soft, leading to no increase in the stiffness due to the presence of hydrate. Two of the results are presented in Fig. 3a, showing consolidation tests with hydrate dissociation conducted by Yoneda et al. (2017) on pressure core sample recovered from the site and the model fitting.

Geomechanical behavior of the mud layer is also simulated by the same constitutive model but with different parameters. There is not enough geomechanical test data for the mud recovered from Site NGHP-02-16. Thus, the clay-rich samples recovered from the Nankai hydrate site, Japan, are used for parameter calibration. Fig. 3b shows the undrained triaxial tests preceded by one-dimensional consolidation on the clay-rich samples from the Nankai site by Nishio et al. (2009) and the fitted model curve. The adopted parameters are summarized in Table 2.

The initial intrinsic permeability for sand is $||\mathbf{K}_0|| = 10^{-12}$ m^2 (1000 mD) and 5×10^{-19} m^2 (0.05 mD) for mud. These values are adopted based on the reservoir-scale model for the site by Myshakin et al. (2017). These values increase/decrease with increase/decrease in the void volume. Some may adopt correlation suggested by Davies and Davies (1999) but in this study, as well as volumetric deformation, the void volume changes with sand migration. Thus, for simplicity, the permeability change is modeled by the incremental form of Kozeny-Carman equation (Kozeny, 1927; Carman, 1937). The effective permeability, which is the permeability with the presence of hydrate, is modeled by

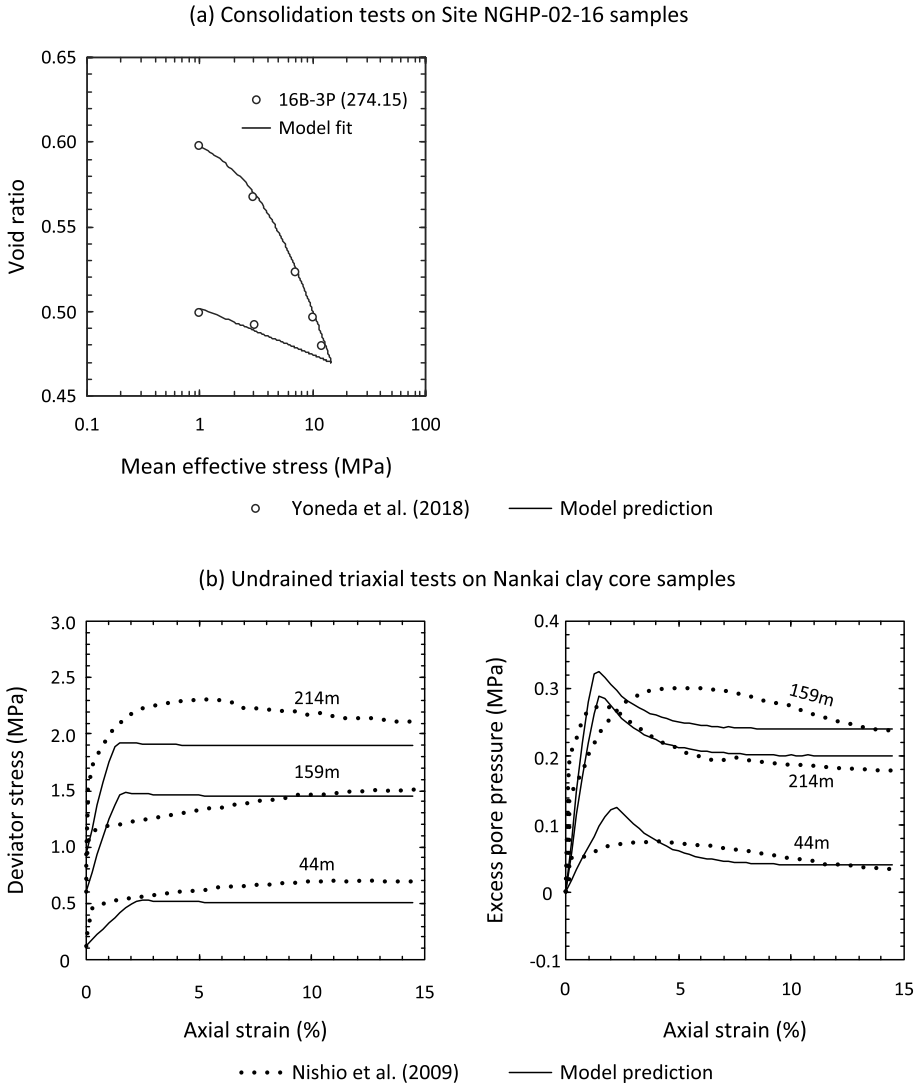

Figure 3: (a) Consolidation tests with hydrate dissociation by Yoneda et al. (2017) and (b) Undrained triaxial tests by Nishio et al. (2009) and the model fitting

using a power law:

$$\mathbf{K}_h = (1 - S_h)^N \mathbf{K} \tag{7}$$

and in this study $N = 4.2$ is used, leading to the initial effective permeability of $||\mathbf{K}_{h0}|| \approx 10^{-15}$ m^2 (1 mD) for the hydrate-bearing sand layer. Eq. (7) states that the effective permeability increases with hydrate dissociation but it is also controlled by the change in the intrinsic permeability. The hydraulic properties are also summarized in Table 2. Other physical properties such as relative permeability relations (van Genuchten, 1980) and the thermal conductivity are presented in Uchida et al. (2016a).

4. Results and discussions

The well pressure decreases to 3.5 MPa (i.e. 25 MPa pressure drawdown) by two days. Under the initial conditions the hydrate phase equilibrium pressure is approximately 20.8 MPa. This means that the hydrates start to dissociate after about 0.6 days into well depressurization. As mentioned previously, the wellbore boundary is open for sand production. In other words, the model does not capture the effect of sand control devices (e.g. screens, gravel packs), thus all migrating sands eventually travel into the well. In order to clarify the effect of the thin mud layer, the analyses also include the cases with only homogeneous hydrate-bearing sand, referred to herein as "sand only".

4.1. Thermo-hydro-mechanical responses

Fig. 4 shows the thermo-hydro-mechanical responses of the hydrate-bearing sand only sediment in near wellbore (consisting of 20 elements in the radial direction from $r = 0.15$ to 4.5 m) at $t = 5$, 10 and 30 days. As expected, depressurization induces hydrate dissociation, dropping the temperature and causing sediment deformation. The volumetric deformation is caused by the increase in the effective stresses due to pore pressure reduction. The deviatoric strain develops as the sediment deforms towards the well, causing shear stressing (i.e. reducing the effective radial stress σ'_r and increasing the effective circumferential stress σ'_θ). In addition, sediment deformation further develops due to reduction in soil strength and stiffness caused by hydrate dissociation. This can be seen by the development of strains from $t = 10$ to 30 days during which the hydrate saturation reduces while the pore pressure remains almost unchanged. Comparing the magnitudes of volumetric and deviatoric strains, it can be said that the sediments deform in more volumetric manner, highlighting the importance of incorporation of volumetric yielding.

Fig. 5 presents the thermo-hydro-mechanical responses of the interbedded hydrate-bearing sediments. Compared with the sand only case (Fig. 4), the presence of a thin mud layer significantly affects the responses of the sediments. Most notably, hydrate dissociation preferentially occurs along the sand/mud layer interface. This is because the mud layer constitutes heat source to drive hydrate dissociation as it remains relatively hotter than the sand layer. As a

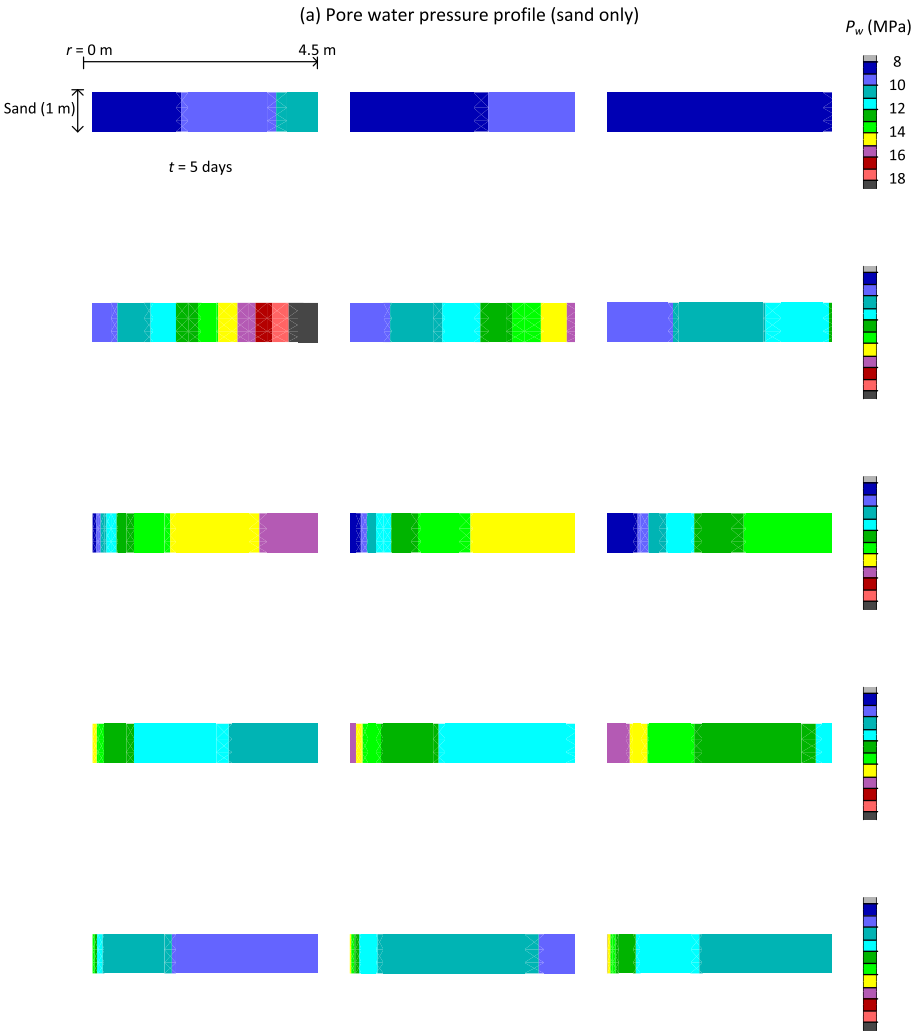

Figure 4: Thermo-hydro-mechanical responses of the hydrate-bearing sand only

result, a larger volumetric strain develops along the sand/mud layer interface. This causes the sediments to deform towards the well as a continuum and thus the sand layer away from the mud layer also deforms in a volumetric manner, effectively increasing the hydrate saturation (by reducing void ratio). This, in return, reduces the permeability in the sand layer, leading to less heat source via convection from far field. As a result, a slower hydrate dissociation away from the mud layer can be observed. This cycle amplifies the preferential hydrate dissociation pattern.

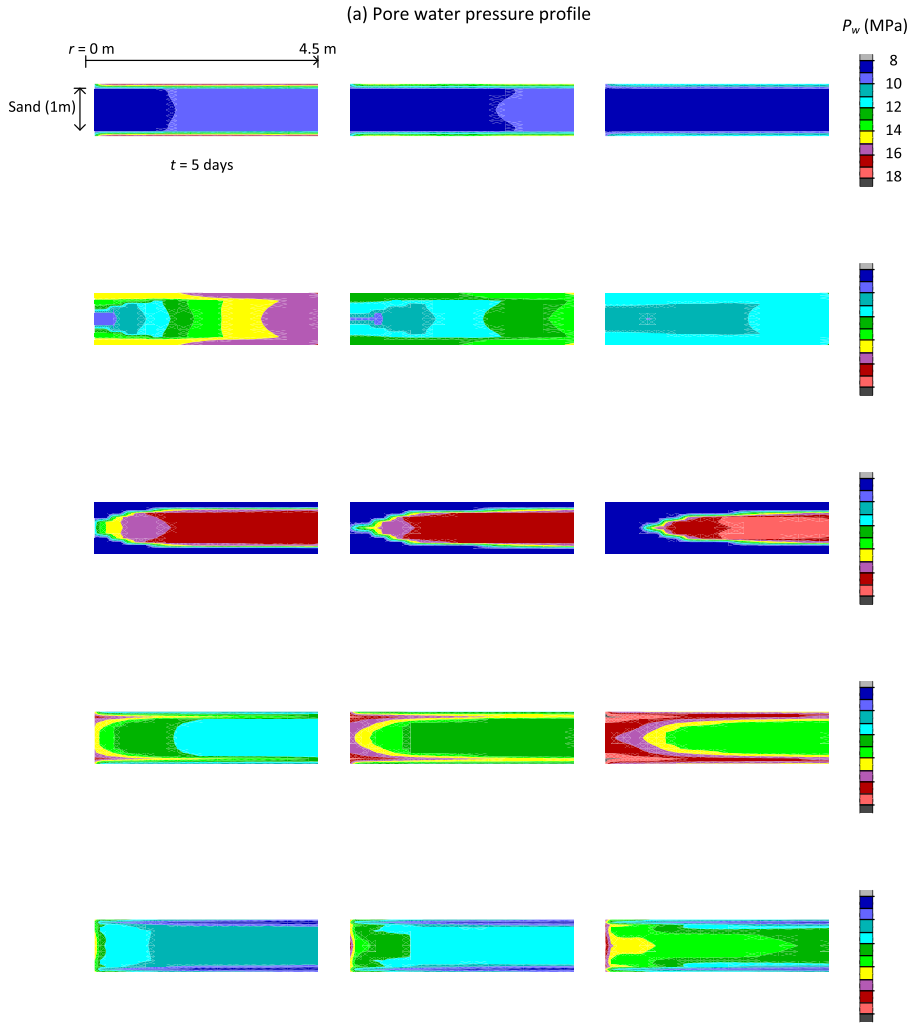

Figure 5: Thermo-hydro-mechanical responses of the interbedded hydrate-bearing sediments

As mentioned previously, hydrate dissociation contributes to sediment deformation. When hydrate dissociates unevenly at a given radius, another important

aspect of mechanical characteristic in hydrate-bearing sediments becomes relevant, that is, hydrate dissociation-induced stress relaxation. Since hydrates in pores carry the applied effective stresses, they temporarily release the effective stresses upon dissociation. The released effective stresses are soon recovered to reach a new stress equilibrium state by deformation, accompanying effective stress development in the neighboring sediments. In other words, sediments with dissociating hydrate pass the effective stresses onto sediments with higher hydrate saturation, causing additional deformation in the sediment with higher hydrate saturation. This unique feature can be found by comparing Fig. 4e and Fig. 5e. Near wellbore, for example, the interbedded sediment shows a greater deviatoric strain by 4 % compared to the hydrate-bearing sand only sediment after it completely loses hydrate (i.e. $S_h = 0$). The difference comes from the fact that the interbedded sediment has carried more effective stresses than the hydrate-bearing sand only sediment and the additional stresses have been transferred from the hydrates onto the neighboring sediments. This difference highlights the importance of rigorous modeling of interbedded sediments to capture heterogeneous nature of hydrate dissociation pattern.

4.2. Sand migration studies

Fig. 6 shows (a) the ratio of hydraulic gradient of water to its critical gradient in logarithmic scale, $\ln(i_w/i_{critw})$; and (b) the volume of detached solids from $t = 0$ to the noted times normalized by the initial solid volume, V_{ssi}/V_{s0}. The positive values in Fig. 6 indicate the areas where detachment can occur and these areas appear to retreat from $r \approx 4.5$ m at $t = 5$ days to $r \approx 2.7$ m at $t = 30$ days. Following two mechanisms contribute to this reduction. One is that the hydraulic gradient is greater in the early stage of depressurization and the other is that hydrate dissociation increases the permeability and in return decreases the hydraulic gradient at a given pressure gradient. Since the hydraulic gradient is always greater than the critical value near the wellbore ($r < 2.0$ m), the volume of detached sands increases with time as shown in Fig. 6b. This is because the shearing deformation keeps developing as hydrate dissociates (as shown in Fig. 4e), increasing the detachability potential as described in Eq. (4). In the middle region (2.0 m $< r <$ 3.6 m) the detached sand volume does not significantly increase because of little development in deviatoric strain. In the areas away from the wellbore (3.6 m $< r$), the detached sand volume remains the same from $t = 5$ days onwards. This is because hydraulic gradient is lower than its critical value. Detailed studies reveal the currently flowing sands at those selected times are negligibly small ($V_{fs}/V_{s0} \approx 10^{-5} - 10^{-4}$), implying the detached sands migrate and flow into a well in a relatively short time.

Fig. 7 shows the sand production related properties in the interbedded hydrate-bearing sediments. Since hydrate dissociation occurs more locally near the sand/mud layers, more detached sands are evident along the sand/mud layers. Detachment is not modeled in the mud layer and thus the detached sands are entirely from the sand layer. The magnitude of detached volume itself is greater compared to the hydrate-bearing sand only case and this is attributed

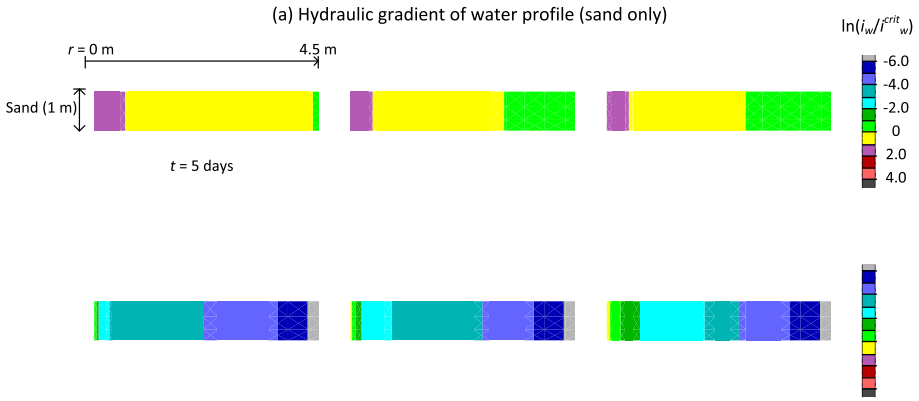

Figure 6: Sand migration related properties in hydrate-bearing sand only

to the greater shearing deformation (values in Fig. 5e > those in Fig. 4e). Detachment does not occur where the hydrates remain in a relatively high amount even though there is detachability potential. This is because hydraulic gradient remains lower than the critical value. However, as the trend suggests, these areas would eventually induce sand particle detachment when the remaining hydrates start to dissociate. Ongoing deviatoric deformation together with the increase in hydraulic gradient, it is likely that detachment of sands continues and expands its areas radially.

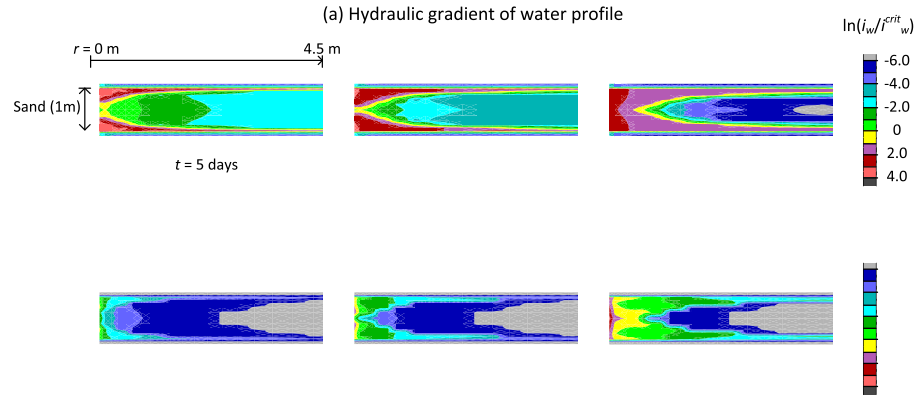

Figure 7: Sand migration related properties in the interbedded hydrate-bearing sediments

In order to understand the durability of sand migration, the history of sand production, that is, the sands that have migrated to the well, is studied. Fig. 8 presents the production of gas, water and sand from a unit height of the well for both hydrate-bearing sand only and interbedded hydrate-bearing sediment cases. It is important to state that by converting the produced volumes in a unit height for the interbedded case (from 1.2 m to 1 m), it effectively reduces

the amount of hydrates in the considered domain but the produced gas volume is greater (Fig. 8a). This shows how beneficial the presence of a thin mud layer is for gas production. In terms of sand production, however, the presence of the mud layer intensifies sand production. While in the hydrate-bearing sand only case, sand production appears to stabilize in the early stage (around 4 days), in the interbedded case it appears to continue even after 30 days as shown in Fig. 8c. The step-wise increase in the produced sand volume is likely to be numerical domain discretization artifact but the rate of sand production over a period of 30 days, that is, approximately 0.05 m^3/m per day, is found to be almost independent of finer/coarser discretization. Although the actual amount of sand production may vary with adopted parameter values, this results show the adverse effect of a thin mud layer on sand production.

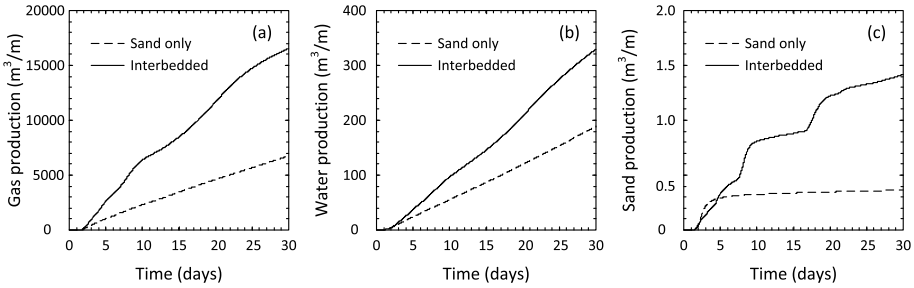

Figure 8: Production of (a) gas; (b) water; and (c) sand over a 30 day period

5. Concluding remarks

This paper presented numerical sand migration modeling of sand/mud interbedded hydrate-bearing sediments at Site NGHP-02-16 subjected to depressurization. The analyses focused on the effect of bounding mud layers on sand production using the coupled thermo-hydro-mechanical sand production model in hydrate-bearing sediments. It was found that greater sand production occurred when the interbedded sand/mud layers were present because of greater shearing deformation and locally high ratios of the hydraulic gradient to the critical gradient along the sand/mud interface. Both mechanisms were attributed to hydrate dissociation and thus it is important to accurately capture the heterogeneous nature of hydrate dissociation pattern. Although the amount of produced sand may vary with selected values of sand production related parameters, this finding implies that there would be a higher risk of sand production if the production zone consists of a large number of sand/mud interbedded layers.

References

Carman, P. C., 1937. Fluid flow through granular beds. Transactions - Institute of Chemical Engineers 15, 150–166.

Dallimore, S. R., Wright, J. F., Yamamoto, K., Bellefleur, G., 2012. Proof of concept for gas hydrate production using the depressurization technique, as established by the jogmec/nrcan/aurora mallik 2007-2008 gas hydrate production research well program, mackenzie delta, northwest territories, canada. Bulletin of the Geological Survey of Canada 601, 1–15.

Davies, J., Davies, D., apr 1999. Stress-Dependent Permeability: Characterization and Modeling. In: SPE Annual Technical Conference and Exhibition. Society of Petroleum Engineers, pp. SPE–56813–MS.
URL http://www.onepetro.org/doi/10.2118/56813-MS

Kozeny, J., 1927. Uber kapillare leitung des wassers in boden. Sitzungsber. Akad. Wiss. Wien 136, 271–306.

Lin, J., Uchida, S., Myshakin, E., Seol, Y., Rutqvist, J., Boswell, R., Waite, W., Jang, J., Collett, T., 2017. Assessing the geomechanical stability of interbedded hydrate-bearing sediments under gas production by depressurization at Site NGHP-02-16. Marine and Petroleum Geology (in this issue).

Myshakin, E., Lin, J., Uchida, S., Seol, Y., Collett, T., Boswell, R., 2017. Numerical simulation of depressurization-induced gas production from an interbedded turbidite hydrate-bearing sedimentary section in the offshore of India: Site NGHP-02-16 (Area-B). Marine and Petroleum Geology (in this issue).

Nishio, S., Ogisako, E., Denda, A., 2009. Geotechnical properties of core samples recovered from seabed ground in East Nankai Trough. Journal of Geography 118 (5), 955–968.

Uchida, S., Klar, A., Yamamoto, K., 2016a. Sand production model in gas hydrate-bearing sediments. International Journal of Rock Mechanics and Mining Sciences 86, 303–316.

Uchida, S., Klar, A., Yamamoto, K., aug 2016b. Sand production modeling of the 2013 Nankai offshore gas production test. In: Energy Geotechnics. Vol. i. CRC Press, pp. 451–458.

Uchida, S., Soga, K., Yamamoto, K., 2012. Critical state soil constitutive model for methane hydrate soil. Journal of Geophysical Research 117 (B3), 1–13.

van Genuchten, M., 1980. A closed form equation for predicting the hydraulic conductivity of unsaturated soils. Soil and Science Society of America Journal 44, 892–898.

Yamamoto, K., Terao, Y., Fujii, T., Terumichi, I., Seki, M., Matsuzawa, M., Kanno, T., May 2014. Operational overview of the first offshore production test of methane hydrates in the Eastern Nankai Trough. In: Offshore Technology Conference. Offshore Technology Conference, Houston, Texas, pp. OTC–25243–MS.

Yoneda, J., Oshima, M., Kida, M., Kato, A., Konno, Y., Jin, Y., Tenma, N., Waite, W., Jang, J., 2017. Consolidation and hardening behavior of hydrate-bearing pressure core sediments under high confining pressure based on natural core sample from NGHP-02. Marine and Petroleum Geology (in this issue).